Manufacturing Technologies and Applications MATECA



Numerical Investigation of the Effects of Using Nanofluid on Thermal Performance and Flow Properties in a Gyroid Structure Heat Exchanger

Gözde Keskin^{1,*} , Gökhan Küçüktürk², Oğuz Turgut²

ABSTRACT

Recently, heat exchangers based on triply periodic minimal surface (TPMS) structures have attracted increasing interest in engineering applications due to their high surface-to-volume ratio, compact design, superior thermal performance, and the feasibility of manufacturing these complex geometries using additive manufacturing technologies. This study, the thermal performance and flow characteristics of a gyroid heat exchanger are numerically investigated using air-air and water-water based Al₂O₃ nanofluids as working fluids. Firstly, the numerical model for the air-air heat exchanger is validated against reference data from the literature for the hot fluid side, then thermal analysis was conducted for at different Re_{cold} numbers. As the Re increased, the heat transfer coefficient, heat transfer and Nusselt number increased. Subsequently, Al₂O₃ nanoparticles were added to the hot-side water base fluid at various volume concentrations (0%, 0.1%, 0.3%, 0.5%), and simulations were conducted under different Re_{hot}-Re_{cold} combinations. It was observed that nanofluid concentration and Reynolds number affected the heat transfer coefficient, heat transfer rate, thermal efficiency and Nusselt number. In addition, a decrease in thermal efficiency was observed with the addition of 0-0.3% nanoparticles, followed by a slight increase between 0.3-0.5%. Studies examining the use of nanofluids in TPMS-gyroid structures are generally limited to heat sink applications; this study provides a contribution to the literature by investigating the effect of nanofluids in a compact cross-flow heat exchanger with simultaneous hot and cold fluid provided.

Keywords: Triply periodic minimal surface, Gyroid heat exchanger, Heat Transfer, Nanofluid

Gyroid Yapıda Bir İsı Eşanjöründe Nanoakışkan Kullanımının İsıl Performans ve Akış Özelliklerine Etkilerinin Sayısal Olarak İncelenmesi

ÖZET

Geleneksel ısı eşanjörlerine kıyasla üçlü periyodik minimal yüzey yapıları kullanılarak tasarlanan ısı eşanjörleri sundukları yüksek yüzey/hacim alanı, kompakt yapıları, üstün ısıl performans kapasiteleri ve eklemeli imalat teknolojisi ile bu özgün yapıların üretilebilirliği nedenleriyle son yıllarda mühendislik uygulamaları için ilgi çekici hale gelmiştir. Bu çalışmada ÜPMY kafes tiplerinden biri olan gyroid yapıda ısı eşanjöründe çalışma akışkanları hava-hava ve su-su bazlı Al₂O₃ nanoakışkanı kullanıldığında ısıl performans ve akış özellikleri sayısal olarak incelenmiştir. İlk aşamada, hava-hava ısı eşanjörü için sayısal model referans literatür sıcak akışkan sonuçlarıyla doğrulanmış, ardından farklı Re_{soğ} sayılarında ısıl analiz çalışması gerçekleştirilmiştir. Sonuçlar Reynolds sayısı arttıkça ısı transfer katsayısının, ısı transferinin ve Nusselt sayısının arttığını göstermiştir. İkinci aşamada, sıcak akışkan su temel akışkanına farklı hacim oranlarında (%0, %0,1, %0,3, %0,5) Al₂O₃ ilave edilmiş ve farklı Re_{sıc}-Re_{soğ} kombinasyonlarında simülasyon çalışmaları gerçekleştirilmiştir. Nanoakışkan konsantrasyonu ve Reynolds sayısının ısı transfer katsayısı, ısı transfer miktarı, termal verimlilik ve Nusselt sayısını etkilediği görülmüştür. Ayrıca termal verimlikte %0-0,3 nanopartikül ilavesinde azalma, bunu takiben %0,3-0,5 arasında bir miktar artış görülmüştür. ÜPMY-gyroid yapılar için nanoakışkan kullanımının incelendiği çalışmalar genellikle ısı alıcı uygulamalarıyla sınırlıdır; bu çalışma ise karşılıklı akışkan geçişinin sağlandığı çapraz akışkanlı kompakt bir ısı eşanjöründe nanoakışkan etkisini inceleyerek literatüre özgün bir katkı sağlamaktadır.

Anahtar Kelimeler: Üçlü periyodik minimal yüzey, Gyroid ısı eşanjörü, Isı transferi, Nano akışkan

1. INTRODUCTION

The primary objective for an efficient design of heat exchanger (HEX) is to enhance the surface area and minimize the pressure drop. Additive manufacturing technology provides significant opportunities for producing of products with complex geometries [1–3]. Triply periodic minimal surface (TPMS) lattice

¹Graduate School of Natural and Applied Sciences, Department of Mechanical Engineering, Gazi University, Ankara, Türkiye

² Department of Mechanical Engineering, Faculty of Engineering, Gazi University, Ankara, Türkiye

^{*}Corresponding author, e-mail: gozdeskeskin@gmail.com

structures have attracted significant interest in HEX design. In minimal surfaces, the sum of the main curvatures at any point is zero. There are numerous researches in which Colburn j-coefficient, heat transfer rate, Nusselt number, pressure drop, and thermal efficiency have been examined for the applications of thermal management systems such as heat sink and HEXs. Peng and al. performed a numerical analysis on a HEX with gyroid TPMS structure for laminar flow using water as the working fluid and fluid velocity of 10 mm/s; they determined that the heat transfer rate was improved by 7.5 times compared to a conventional plate HEX [4]. Liang et al. investigated the heat transfer and flow characteristics of a cross-flow HEX designed with gyroid, S-D and diamond type core structures with 82% porosity, experimentally and numerically. The working fluid was air on both sides and the experimental study was carried out at Re_{hot}=2300-8900 and Re_{cold}=2300-4800. As a result, it was observed that both the heat transfer rate and the heat transfer coefficient increased as the Reynolds number increased. However, the performance decreased until reaching the Rehot=4500, and then began to increase [5]. In another study, the effects of changing the cell unit size on heat transfer for a HEX designed with S-D structure and the same porosity percentage were investigated. They stated that reducing the unit size improved the HEX performance by at least 10%, but may cause a pressure loss of 40% [6]. Tang et al. investigated the heat transfer properties for the heat sink consisting of gyroid, diamond and Iwp TPMS lattice structures depending on the air flow rate and numerically compared the results with the conventional fin type heat sink. Thermal efficiency decreased in the order of Diamond>Gyroid>Iwp>Fin. The simulation study was experimentally validated laminar and turbulent flow in the range of Re_{cold}=135-3500 for the gyroid structure. Comparative numerical study was carried out in the range of Re_{cold} =166-943 [7]. Barakat et al. conducted a numerical analysis study specific to the Fischer Koch-S (FKS) lattice model and investigated its heat transfer properties. They compared their results with gyroid, diamond, Split-P lattice structures. In the investigation performed for the air cooling system, they stated that the heat transfer coefficient and Nu number values of the FKS lattice were higher compared to other TPMS lattice structures, but it has the drawback pressure drop at high Reynolds numbers [8]. In other research, Barakat et al. proposed a mathematical parameter to control the deformation for diamond and gyroid lattice structures, and numerically examined its effects as a function of Reynolds number [9]. Samson et al. investigated the effects of porosity and cell size as geometrical design parameters on thermal performance and flow characteristics for a gyroid heatsink under turbulent flow, by comparing it with a fin heatsink. Approximately 300% increase in Nusselt number and 42% increase in performance were observed [10]. Barakat et al. performed numerical and experimental studies for the optimization of cell periodicity, radius design parameters and heat transfer properties of Diamond, Gyroid, SplitP and Lidinoid TPMS models [11]. Mahmoud et al. investigated the effect of cell size, thickness and aspect ratio on the thermal performance of a cross-flow gyroid HEX with air-liquid working fluids and examined their relationship with pressure drop [12]. Samad et al. investigated the heat transfer performance of gyroid HEXs with equal and unequal flow channels based on experimental and computational analysis. They stated that the heat transfer coefficient of gyroid HEX with unequal flow channel, where the working fluid is liquid-liquid, is higher than the equal flow channel, and the smaller cell size enhances the heat transfer properties due to the increase in surface area [13]. In the study performed by Kilic, an experimental and numerical study was carried out in turbulent flow for a gyroid HEX containing water-0.6% nanoparticles. They stated that the use of nanofluid increases the temperature distribution by 8-12% compared to distilled water [14]. It has been observed that in the studies in the literature examining the heat transfer properties of TPMSbased HEXs and heatsinks, the focus is generally on air-air, air-liquid and liquid-liquid flows for working fluids. For instance, Liang et al. [5,6] investigated air- air flow, Samad et al. [13] examined water-water flow in HEX and Kilic [14] focused on a TPMS based cooling system using nanofluid under single fluid flow without cross flow interaction. In this study, thermal performance and flow properties of air-air and Al₂O₃water nanofluid flow (liquid-liquid) at different volumetric ratios (%0; 0.1; 0.3; 0.5) for a HEX designed with a gyroid structure, one of the triply periodic minimal surface types, were numerically investigated for different Reynolds numbers. Unlike previous studies, this study aimed to investigate the heat transfer and flow properties of nanofluids in a cross-flow gyroid HEX and to investigate the effects of nanoparticle addition. A review of the literature shows that, it is seen that there are limited studies examining the effect of using nanofluid as a working fluid on thermal performance and flow properties in HEXs and heatsink with TPMS structures. Therefore, it is thought that the analysis data obtained from this research will contribute to the literature.

2. THEORETICAL MODEL

2.1. Creation of the Geometric Model

In heat exchanger design, basic requirements such as operating temperature and pressure, thermal efficiency, fouling and pressure drop must be taken into account. In order to meet these requirements, determining the surface area/volume ratio at the optimum level is of great importance [4]. On the other hand, the conditions for manufacturability with additive manufacturing methods also play a critical role in maintaining structural integrity and achieving a production success free of voids or manufacturing errors. Therefore, in this study, design parameters were determined by taking existing application examples in the literature as reference, such as Liang et al. [5], who used similar porosity and cell size in a TPMS-based design. A gyroid HEX model with 82% porosity was created in the dimensions of $48 \times 16 \times 48$ mm in .stl file format using the nTopology software [15]. While creating the geometry, the inlet and outlet surfaces were closed with a thin wall so that the cold and hot fluids could pass through the flow channels without mixing with each other. The unit cell size of the gyroid is 16 mm and it is arranged in 3x1x3 units. The implicit equation of the gyroid TPMS structure is given as follows [7,16]:

$$cos(x)sin(y) + cos(y)sin(z) + cos(z)sin(x) = 0$$
(1)

The geometry was created in nTopology through the following steps: Firstly, a design area of 48x16x48 mm and 4 covers of 48x16x1 mm were created through the "box" command. TPMS walls; rectangular volume lattice was defined in the design area from the "unit cell" and "unit cell size" commands. Gyroid was selected as the unit cell type, and a unit cell size of $16 \times 16 \times 16$ mm was defined. Approx. thickness was entered as 1.38 mm. Then "TPMS cold fluid" was created from the "periodic lattice" command. Here, the unit cell was defined as a TPMS unit cell with offset; the cell map was set to rectangular cell map, and the midsurface offset was defined. In order to create "TPMS hot fluid", primary body: design area and subtraction bodies are defined as "boolean subtract" command: TPMS walls and TPMS cold fluid were selected. Then 4 baffles were created in order. With the help of the "boolean intersect" command, the process was repeated with the "intersect" command option of 48x16x1 mm boxes, TPMS hot fluid and TPMS cold fluid. Subsequently, for the hot fluid, 2 baffles were subtracted from the TPMS cold fluid by means of the "boolean subtract" command. For the cold fluid, the other 2 baffles were subtracted from the hot fluid by means of the "boolean subtract command". Thus, hot and cold fluid volumes can be created.

The representative illustration of the prepared geometric model is presented in Figure 1. Subsequently, surface meshing and repair operations were performed to prepare the model for computational fluid dynamics (CFD) analysis. The calculated domain is the 48x16x48 mm slice of the geometric volume with dimensions of 96x48x96 mm. It is assumed that the wall regions other than the gyroid structure do not affect the flow profile. By adding 30 mm long extension sections to the inlet and outlet boundaries of the calculation area, it is aimed to see the flow profile formed at the inlet and outlet sections.

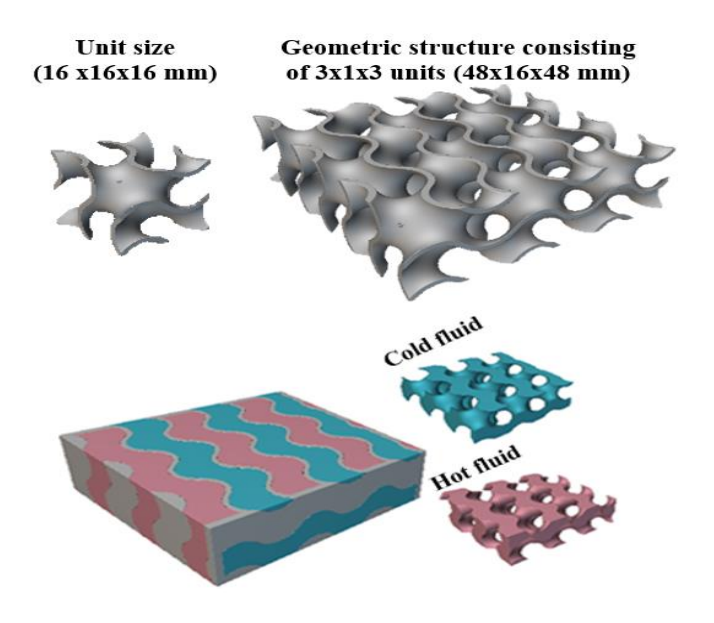


Figure 1. Modeling of the structure in nTopology.

2.2. Equations Used in the Study

2.2.1. Heat Transfer Calculations

The following equations were used in the numerical analysis [5,6]. Heat transfer due to fluid's temperature difference:

$$Q = \dot{m} c_p |T_i - T_o| \tag{2}$$

Here, \dot{m} is the mass flow rate, c_p is the specific heat capacity, T_i is the inlet temperature and T_o is the outlet temperature, respectively. The thermal efficiency " \mathcal{E} " of the HEX is calculated from the ratio of the average heat transfer (W) to the maximum heat transfer value as follows.

$$Q_{avg} = \frac{Q_{hot} + Q_{cold}}{2} \tag{3}$$

$$\varepsilon = \frac{Q_{avg}}{Q_{maximum}} = \frac{Q_{avg}}{(\dot{m} c_p)_{min}(T_{i,hot} - T_{i,cold})}$$
(4)

The heat transfer coefficient is calculated as follows.

$$U = \frac{Q_{avg}}{LMTD \ x \ A} \tag{5}$$

Here LMTD is the logarithmic temperature difference and is calculated as follows.

$$LMTD = \frac{\left(T_{i,hot} - T_{o,cold}\right) - \left(T_{o,hot} - T_{i,cold}\right)}{ln\left(\frac{T_{i,hot} - T_{o,cold}}{T_{o,hot} - T_{i,cold}}\right)}$$
(6)

The Reynolds number is calculated as follows using the inlet flow rate and hydraulic diameter.

$$Re = \frac{\rho V D_h}{\mu} \tag{7}$$

Here D_h is the hydraulic diameter, μ is the dynamic viscosity, and V is the average flow rate at the flange inlet. D_h is the hydraulic diameter equal to 4 times the ratio of the area to the perimeter at the flange inlet. The Nusselt number is calculated as follows:

$$Nu = \frac{U \times D_h}{K} \tag{8}$$

Here K represents thermal conductivity.

2.2.2. Thermophysical Properties of Water-Al₂O₃ Nanofluid

The addition of nanoparticles to the base fluid changes the thermophysical properties of the fluid. Variations in density, dynamic viscosity, specific heat capacity and thermal conductivity are observed. The density, dynamic viscosity, specific heat capacity and thermal conductivity parameters of the water-Al₂O₃ nanofluid are calculated using the formulas presented in Equation (9-12) [17,18]:

$$\rho_{nf} = (1 - \varphi)\rho_{bf} + (\varphi)\rho_{p} \tag{9}$$

$$\mu_{nf} = \mu_{bf}(1 + 2.5 \,\varphi) \tag{10}$$

$$c_{p,nf} = (1 - \varphi)c_{p,p} + (\varphi)c_{p,bf} \tag{11}$$

$$K_{nf} = K_{bf} \frac{K_p + 2K_{bf} - 2(K_{bf} - K_p)\varphi}{K_p + 2K_{bf} + 2(K_{bf} - K_p)\varphi}$$
(12)

Here, subscripts "p" refers to the the nanoparticle and "bf" represents the base fluid (water). ϕ is the volume fraction of the nanoparticle in the nanofluid.

In this study, Al_2O_3 nanoparticles were added to the water base fluid. Air was used as the reference fluid in the validation study. The inlet temperature of the cold fluid $T_{i,cold}$ =293 K and the inlet temperature of the hot fluid $T_{i,hot}$ =333 K. The thermophysical properties of air, water and Al_2O_3 nanoparticles are presented in Table 1.

	ρ (kg/ m ³)	μ (kg/m.s)	C _p (J/kg.K)	K (W/m.K)
Air (333 K)	1.060	1.9987x10 ⁻⁵	1007	0.02808
Air (293 K)	1.204	1.8127x10 ⁻⁵	1007	0.02514
Water (333 K)	983.2	46.7x10 ⁻⁵	4183	0.641
Water (293 K)	998.2	100.2x10 ⁻⁵	4183	0.5861
Al_2O_3	3900	_	842.95	33.58861

Table 1. Thermo-physical properties of air, water and Al₂O₃ nanoparticles [19,20].

3. NUMERICAL ANALYSIS

The numerical simulation study was carried out using ANSYS CFX software, applying periodic boundary conditions on the top and bottom surfaces, by using the shear stress transport turbulence model $(k-\omega)$ in three dimensions under steady-state conditions. Shear Stress Transport (SST) k- ω turbulence model was selected to predict flow behavior in complex geometries with high curvature and flow separation such as TPMS based gyroid structures. This model especially suitable for capturing both boundary layer evolution and bulk flow behavior. Additionally, this model provides improved accuracy in channel flows and porous structures compared to k- ε model [5,6,8,9,21]. Also, in air–air analyses, ideal gas assumption and Sutherland's viscosity model were used to obtain values closer to experimental results [22]. For the liquid-liquid side, incompressible flow and constant viscosity assumptions were assumed. These assumptions were made to reduce the computational load and optimize the solution time of the model. The mesh structure was generated with tetrahedral elements using ANSYS Meshing. ANSYS Meshing. In order to ensure the numerical accuracy in the boundary layer (at the fluid-solid interface) and to maintain that the y+ values around 1, a boundary layer cell consisting of a first layer height of 0.025 mm, a growth rate of 1.2 and 13 layers was formed near the solid wall (Figure 2). The boundary conditions of the model are defined as T_{i,hot}=333 K, T_{i,cold}=293 K, atmospheric pressure at the outlet, thermal conductivity of the aluminium wall 181 W/(m-K). Analyses were performed using a constant velocity inlet, corresponding to Reynolds numbers in the range of Rehot=2300-4500 and Re_{cold}=2500-4500. Thermal performance and flow properties for the combinations of Re_{cold}=2500, 3500, 4500 and Rehot=2300,3000,3900,4500 for the air-air flow; and for the liquid-liquid flow, with the addition of Al₂O₃ nanoparticles to the hot fluid at different volume fractions (%0;0.1;0.3;0.5) and combinations of Rehot=2500, 3500, 4500 and Re_{cold}=2500,4500 were investigated. Figure 3 shows the details of the numerical model.

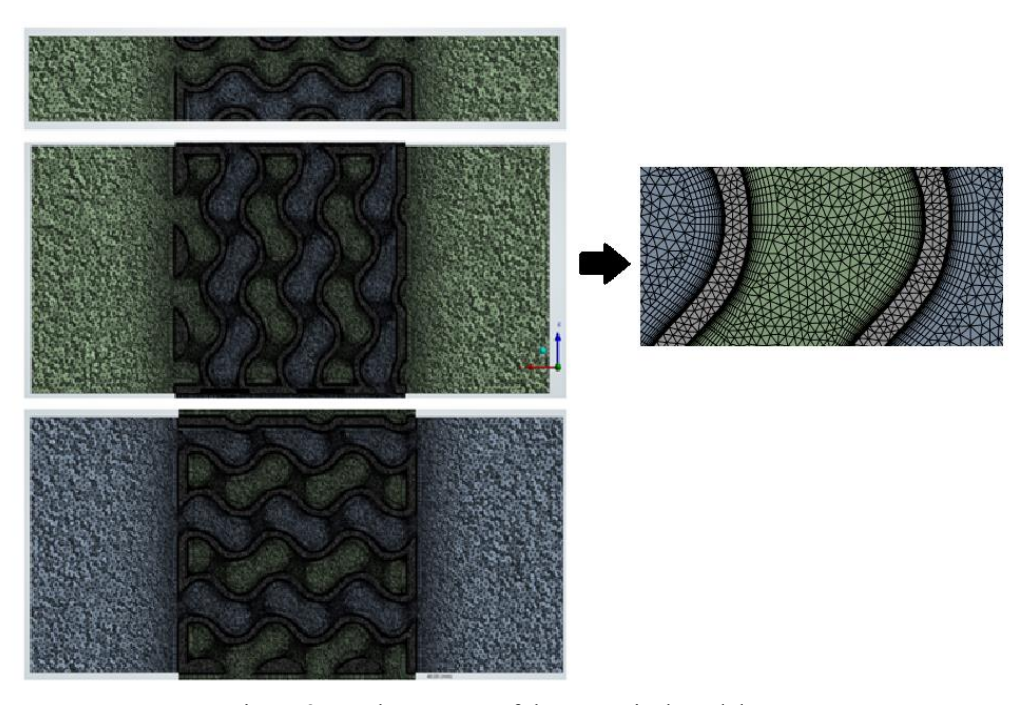


Figure 2. Mesh structure of the numerical model.

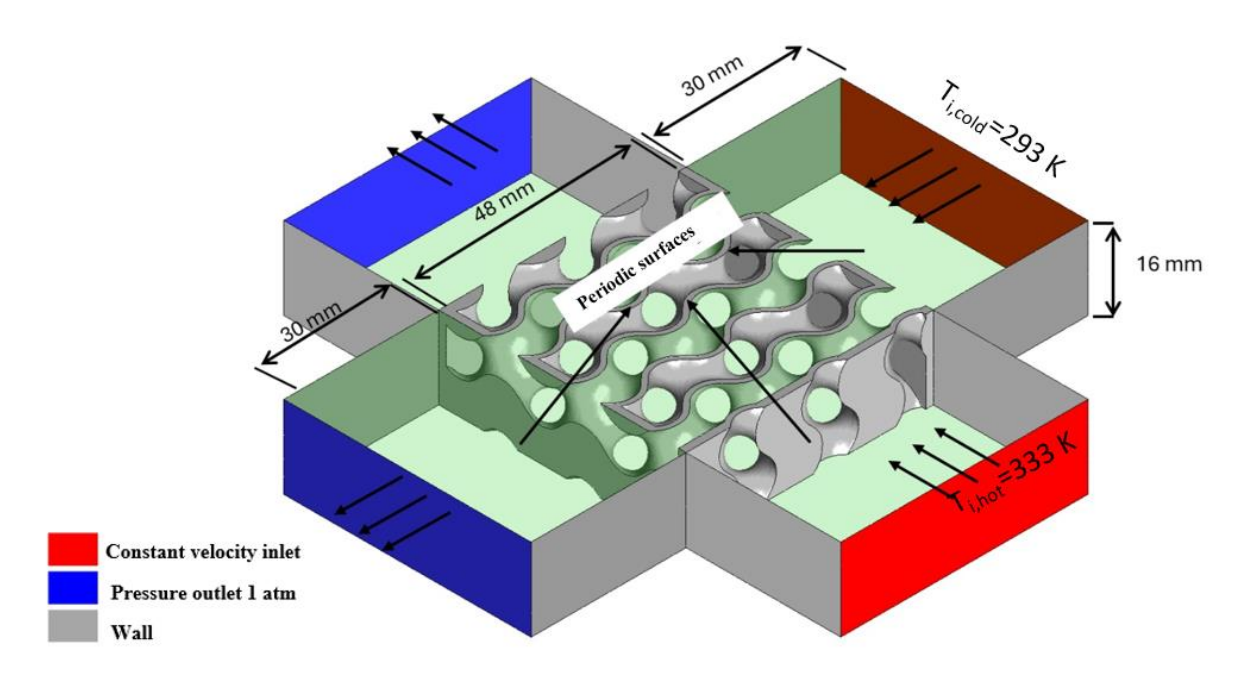


Figure 3. Physical model geometry.

3.1. Validation of the Numerical Study

For the validation of the numerical study, the simulation model and experimental data of Liang et al. in the literature were used as references [5]. Liang et al. investigated the design and fabrication of HEX based on gyroid, SD, primitive structure and evaluated their heat transfer and flow properties under high Reynolds number, both numerically and experimentally. The production geometry and dimensional properties of the HEX used for testing in the literature study are; core section is 96x64x96 mm, unit cell size is 16 mm and relative density is 18%. The cold side flow rate kept constant, while the hot flow side conditions are varied for different cell types (gyroid, S-D and primitive) of HEX at Reynolds numbers ranging between 2300 and 8900 and the results are reported. Due to the computational cost and geometry complexity, the simulation study was carrried out for 48x16x48 mm by simplifying the geometry. In the simulation model, the HEX hot air inlet temperature is 333 K, cold air inlet temperature is 293 K, the thermal conductivity of the solid area, namely

the gyroid wall, is 181 W/m K aluminum alloy, and the fluid is specified as ideal gas. The boundary condition is assumed to be atmospheric pressure (1 atm) at the outlet and periodic at the top and bottom surfaces. Mesh independence evaluation is applied to ensure that simulation results are independent from the number of elements. Numerical analysis was performed for the cold and hot fluid at Re=4500 under the above mentioned simulation model conditions. The optimal mesh was determined by examining the variation in the results depending on the number of mesh elements. As seen in Table 2, the pressure drop and heat transfer coefficient results were examined for 2.85 (mesh-1), 4.54 (mesh-2), 6.55 (mesh-3), 10.7 (mesh-4), 13.3 (mesh-5) and 19.02 (mesh-6) million mesh elements. Considering the change in pressure difference (ΔP) and heat transfer coefficient (U) values less than 1 percent and the calculation cost in the transition from 13.3 million element number to 19.02 million element number, the optimal element number was determined as 13.3 million. Therefore, in the validation study, the mesh size and settings of 13.3 x 10^6 were applied in the calculations in the current study.

#Mesh No:	1	2	3	4	5*	6
Number of	2.85×10^6	4.54×10^6	6.55×10^6	10.7×10^6	13.3 x10 ⁶	19.02 x10 ⁶
mesh elements						
U (W/ m ² ·K)	40.925	42.43	42.642	43.054	43.2	43.384
Error (%)	-	3.68	0.49	0.97	0.35	0.41
$\Delta P (Pa)$	56.24	58.5	59.33	58.67	59.18	59.43
Error (%)	-	4.01	1.41	1.1	0.87	0.42

Table 2. Mesh independence study

In order to validate the numerical solution, firstly, the analysis was performed in the combinations of Re_{hot} =4500, Re_{cold} =4500 and Re_{cold} =4500, Re_{hot} =8900. The simulation and experimental results of Liang et al. [5] and the current numerical solution results are presented in Figure 4. It was found that the difference with the experimental results is about 6.3% and the difference with the numerical results is about 4% in the condition of Re_{hot} =4500, Re_{cold} =4500. It was observed that the difference with the experimental results is about 13% and difference with the numerical results is about 3.7% in the condition of Re_{hot} =8900, Re_{cold} =4500.

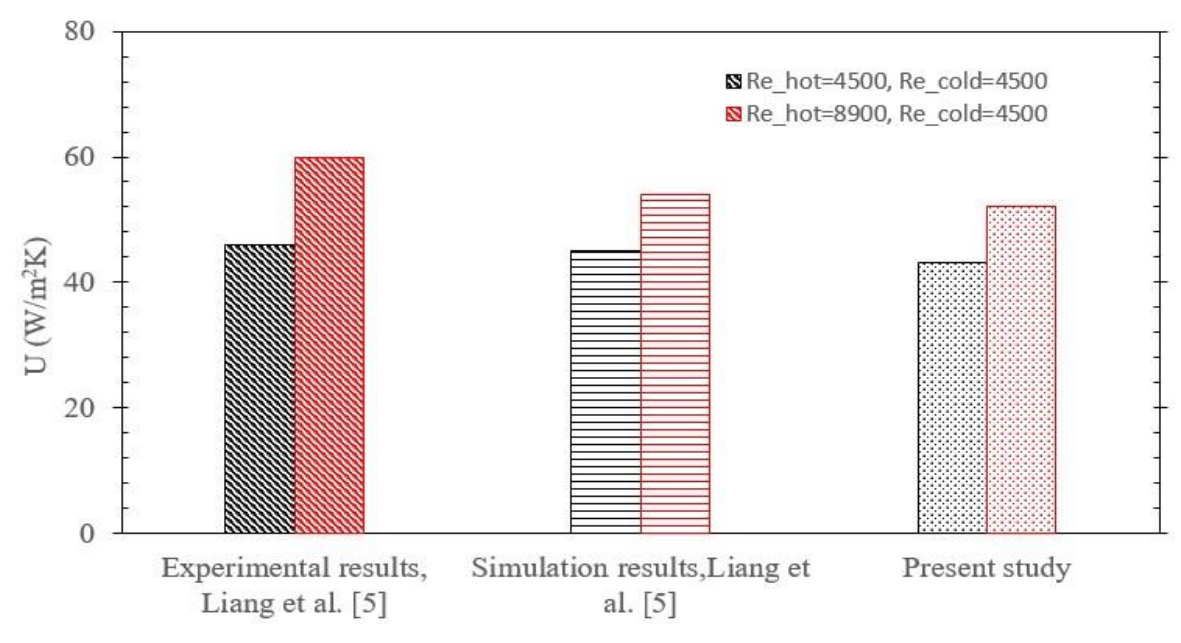


Figure 4. Comparison of the heat transfer coefficient values obtained from the simulation results.

Then, the experimental results of Liang et al. [5] were compared with the U values for different values in the range of Re=2300-9000 in the current study. It was evaluated that the deviation percentage results ranging from 3.4 % to 13.3 % were consistent. In the simulation study, an increase in the deviation was observed after approximately Re_{hot}=7000. In Figure 4, the deviation was found as 11 % for Re_{hot}=8900 and Re_{cold}=4500 in the experimental study of Liang et al. [5]. In this Re combination, it was observed that the difference with the experimental results was approximately 13. This indicates that the percentage difference in deviation is within acceptable range.

It is evaluated that the reason for the differences in the experimental and numerical studies are resulting from various factors: the roughness values of the HEX produced with the additive manufacturing method or any manufacturing errors, which were not taken into account in the numerical study; the complexity of the geometry and the cost of CFD analysis; the simulation model is scaled as 1/16th of the main model used in the experiment in terms of volume; the deviations of the measurement device used in the experimental setup; environmental effects and uncertainties that may occur in the experiments cannot be reflected in the simulation; and the effect of the U and ϵ uncertainties which were reported as approximately 7% in the reference study.

Since the deviation remained below 5% up to Re=4500 in the simulation study, Re_{hot}= 4500 was determined as the limit in the numerical analysis study to be carried out within this scope.

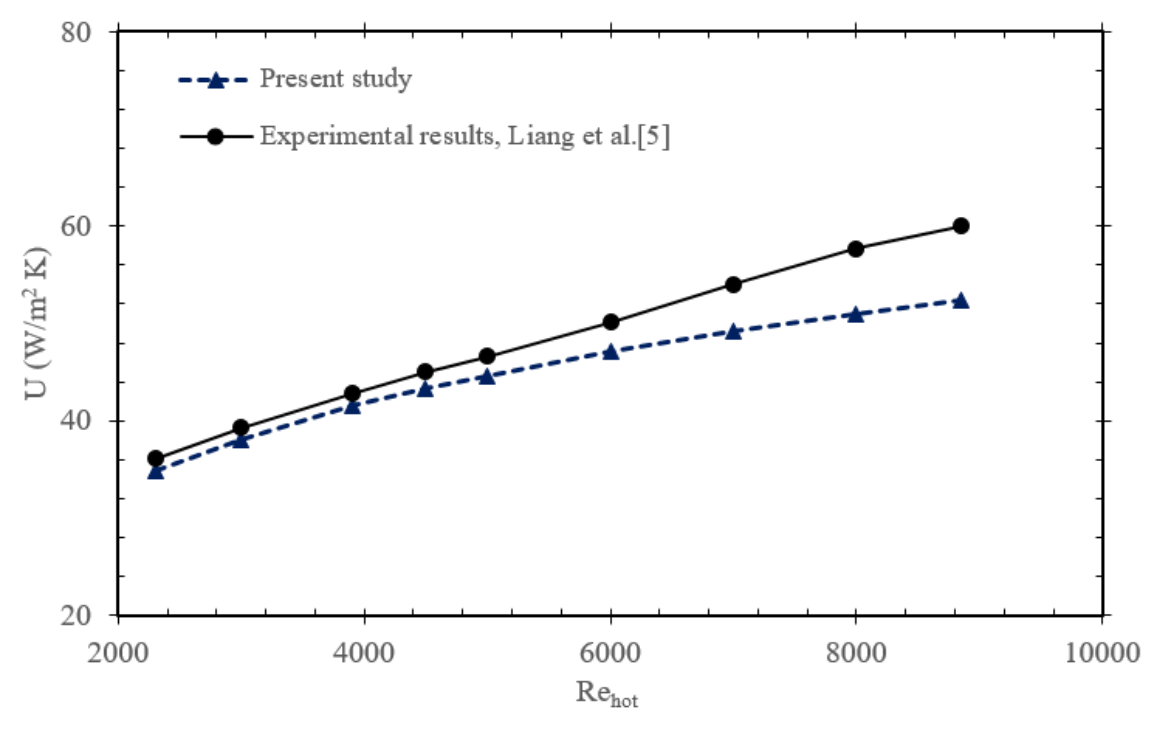


Figure 5. Comparison of heat transfer coefficient values between simulation results and experimental results.

4. RESULTS AND DISCUSSION

4.1. Influence of Cold Fluid Reynolds Number Variation on Thermal Performance

In this study, the heat transfer performance of the cold fluid at different Reynolds numbers ($Re_{cold}=2500$, 3500, 4500) was evaluated. Thus, the effect of the cold side flow rate change on U, Q, ϵ and Nusselt number in a cross-flow thermal system was analyzed. When Figure 6 and Figure 7 are examined, an increase in Re on the hot fluid side results in a significant increase in both Q and U values. On the other hand, for the cold fluid side, increasing Re_{cold} at various Re values led to an increase in U and Q parameters in each hot fluid regime. That is, not only the hot fluid but also the cold fluid plays a critical role in thermal performance. The highest heat transfer was obtained at the conditions of $Re_{hot}=Re_{cold}=4500$. When the thermal efficiency graph in Figure 8 is examined, it is seen that the thermal efficiency of the HEX decreases as the Re_{hot} increases. As Re increases, despite the increase in Q, the mass flow rate of the passing hot fluid also increases, therefore the inlet and temperature difference of the hot fluid is less. When the (mcp)_{hot} value is smaller than the (mcp)_{cold} value, the thermal efficiency formula given by Equation 4 is simplified as follows [5]:

$$\varepsilon = \frac{T_{i,hot} - T_{o,hot}}{T_{i,hot} - T_{i,cold}} \tag{13}$$

As stated in the literature, when $(\dot{m}c_p)_{hot} > (\dot{m}c_p)_{cold}$, the thermal efficiency decreases [5]. The maximum performance was achieved under conditions $Re_{hot}=2300$, $Re_{cold}=4500$. As seen in Figure 9, the maximum Nu value was observed when Re_{hot} and Re_{cold} values were 4500. The graph presents the change in Nu number for different values of Re_{cold} as Re_{hot} increases. As Re_{hot} increases, Nu increases, and as Re_{cold} increases, there is

an increasing trend in Nu values for each Re_{hot} value. This is due to the improvement in heat transfer as turbulence intensity increases.

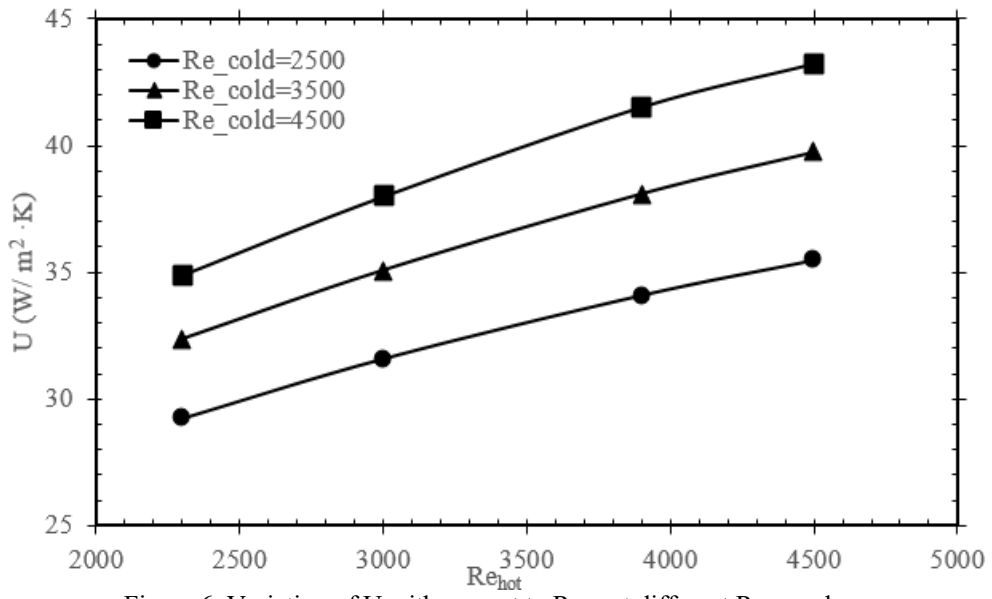


Figure 6. Variation of U with respect to Re_{hot} at different Re_{cold} values.

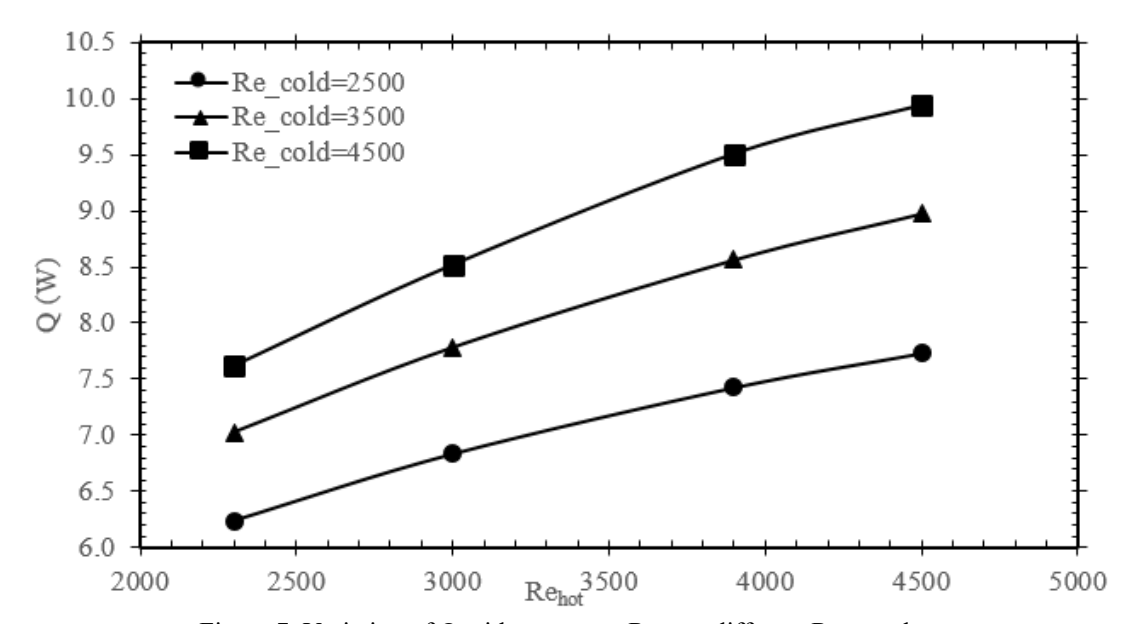


Figure 7. Variation of Q with respect to Re_{hot} at different Re_{cold} values.

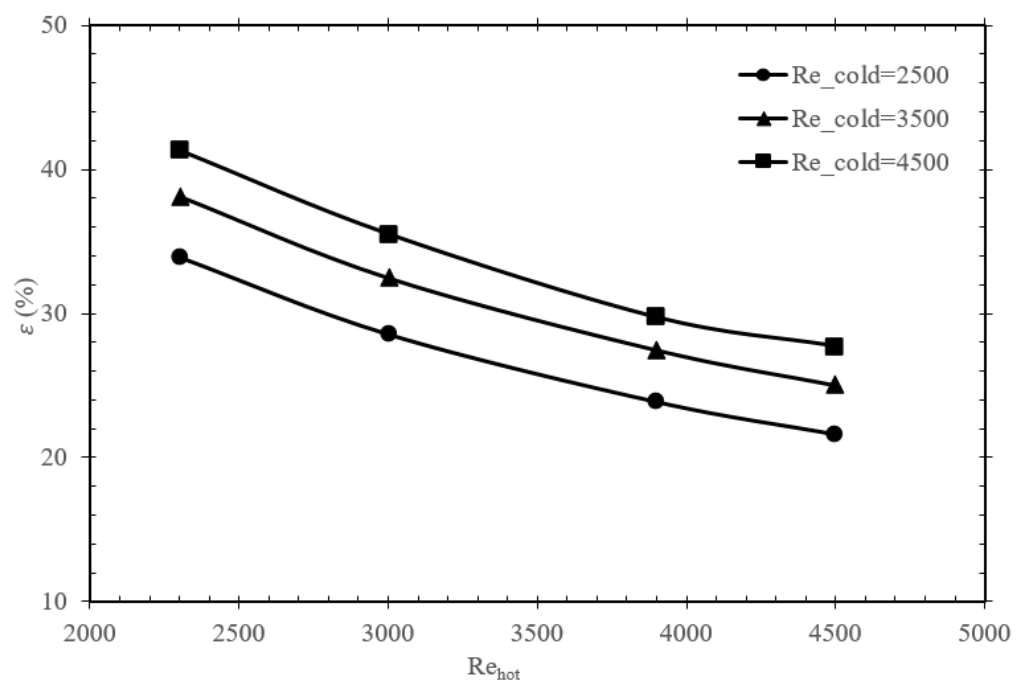


Figure 8. Variation of ε with respect to Re_{hot} at different Re_{cold} values.

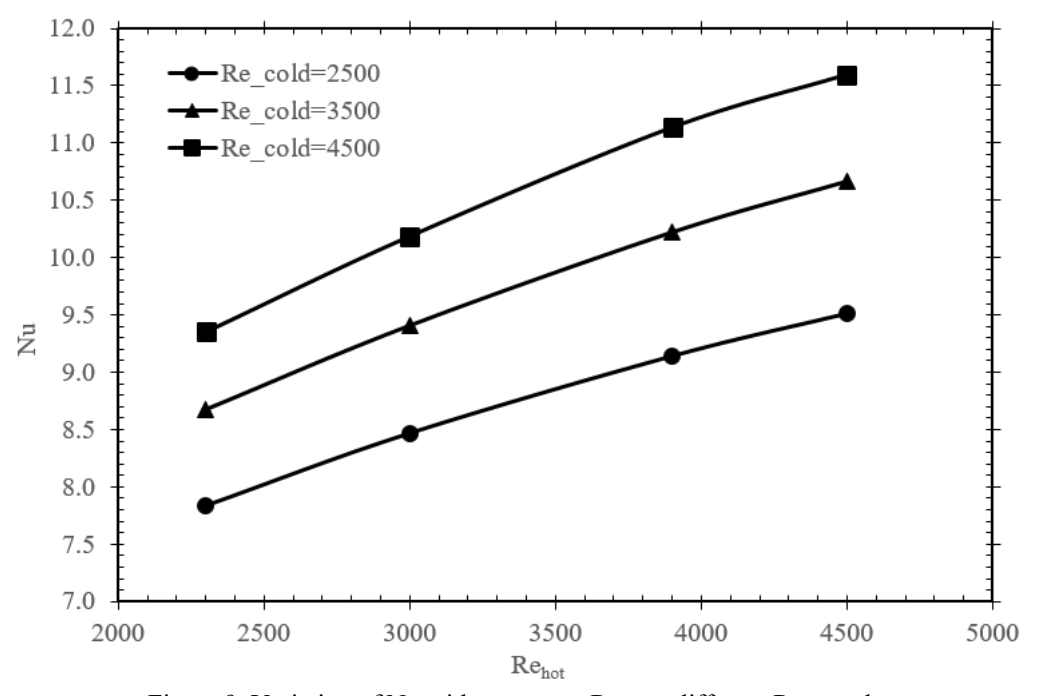


Figure 9. Variation of Nu with respect to Rehot at different Recold values.

4.2. Thermal Performance Evaluation of Al₂O₃-Water Nanofluid

In this section, Re_{hot} was set to 2300, 3500 and 4500, and the nanoparticle volume fraction (ϕ) was changed between 0% and 0.5%. For the cold fluid side, comparative analyses were performed by keeping the Re number constant as 2500 and 4500, respectively. Heat transfer and flow performance were evaluated according to different Re values and nanoparticle ratios on both fluid sides. Figure 10 shows the variation of the U with respect to Re number and ϕ . At a constant $Re_{cold} = 2500$, the increase in ϕ in the hot fluid results in a limited increase in U at the same Re values of the hot fluid. When $Re_{cold} = 4500$ and the hot fluid has the same Re number, the increase in U becomes more noticeable at 0.3% and 0.5% with increasing ϕ . It can be evaluated that the addition of nanoparticles increases the Reynolds number by increasing both the thermal conductivity of the hot fluid and the heat flux at the fluid-wall interface. As shown in Figure 11, the U graph is plotted as a function of increasing ϕ at varying hot fluid Reynolds numbers for the cold fluid side $Re_{cold} = 2500$ and $Re_{cold} = 4500$. It was observed that in all Re combinations, increasing the ϕ caused an increase in U. At 0.5%

nanofluid percentage and hot fluid Re_{hot}=4500, U increased by 15.6% when the cold fluid Re number increased from 2500 to 4500. It can be concluded that the flow regime, particularly the increase in turbulence intensity and higher flow velocity, directly influences U.

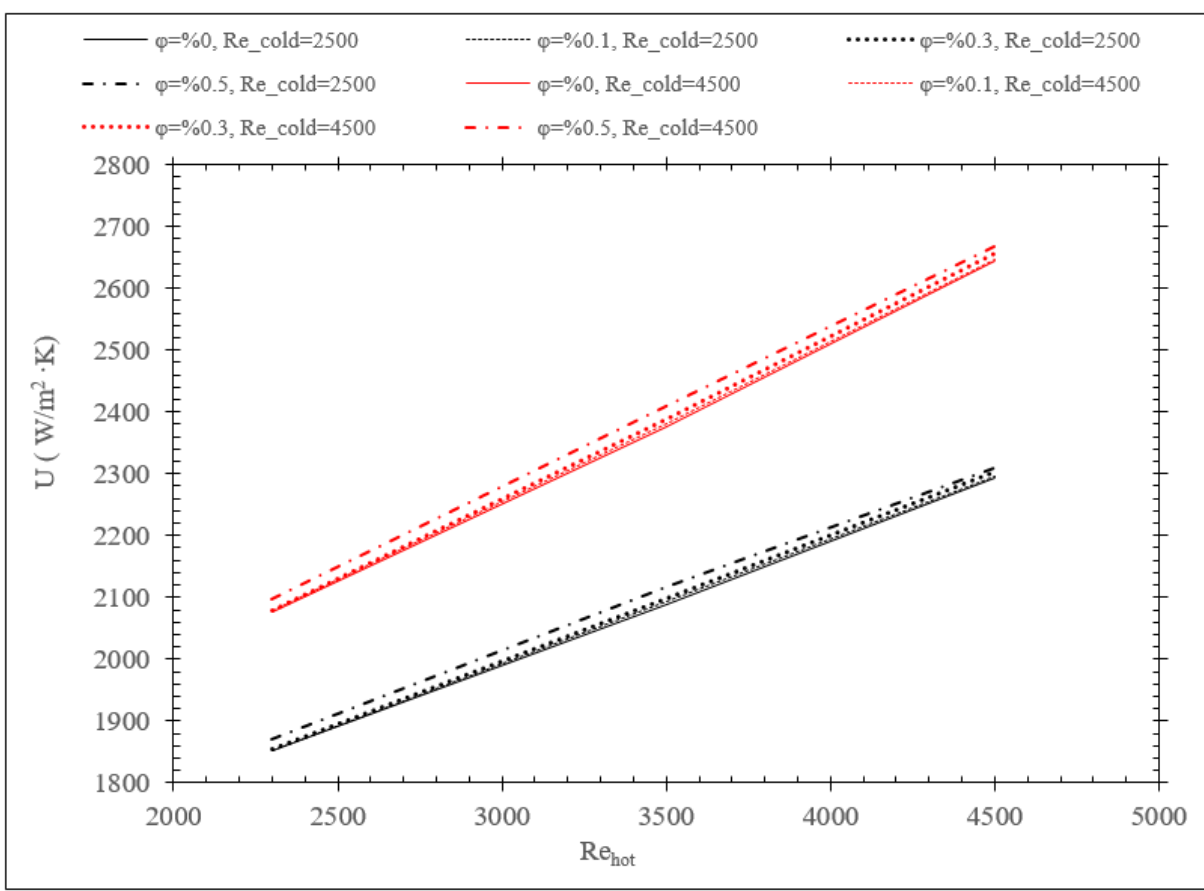


Figure 10. Effect of Reynolds number on heat transfer coefficient in Al₂O₃ nanofluid.

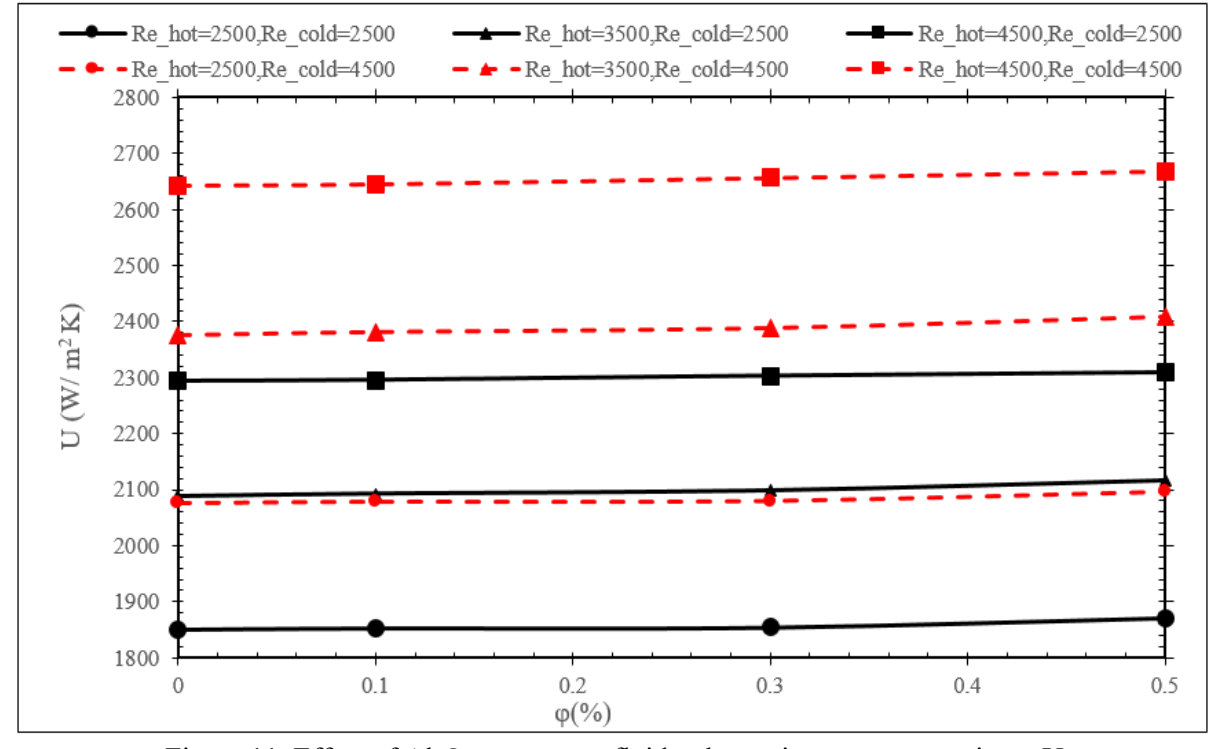


Figure 11. Effect of Al₂O₃-water nanofluid volumetric percentage ratio on U.

The effect of the Al_2O_3 -water nanofluid volumetric percentage ratio and Reynolds number on Q is presented in Figure 12. As the Al_2O_3 volumetric concentration and Reynolds number of both hot and cold fluids increase, an enhacement in the Q is observed. When the ϕ =0.5% and Re_{hot} =4500, it is observed that the Q increases by 17.1% as the Re_{cold} increases from 2500 to 4500. This can be interpreted ad the result of increased flow rate enhancing Q.

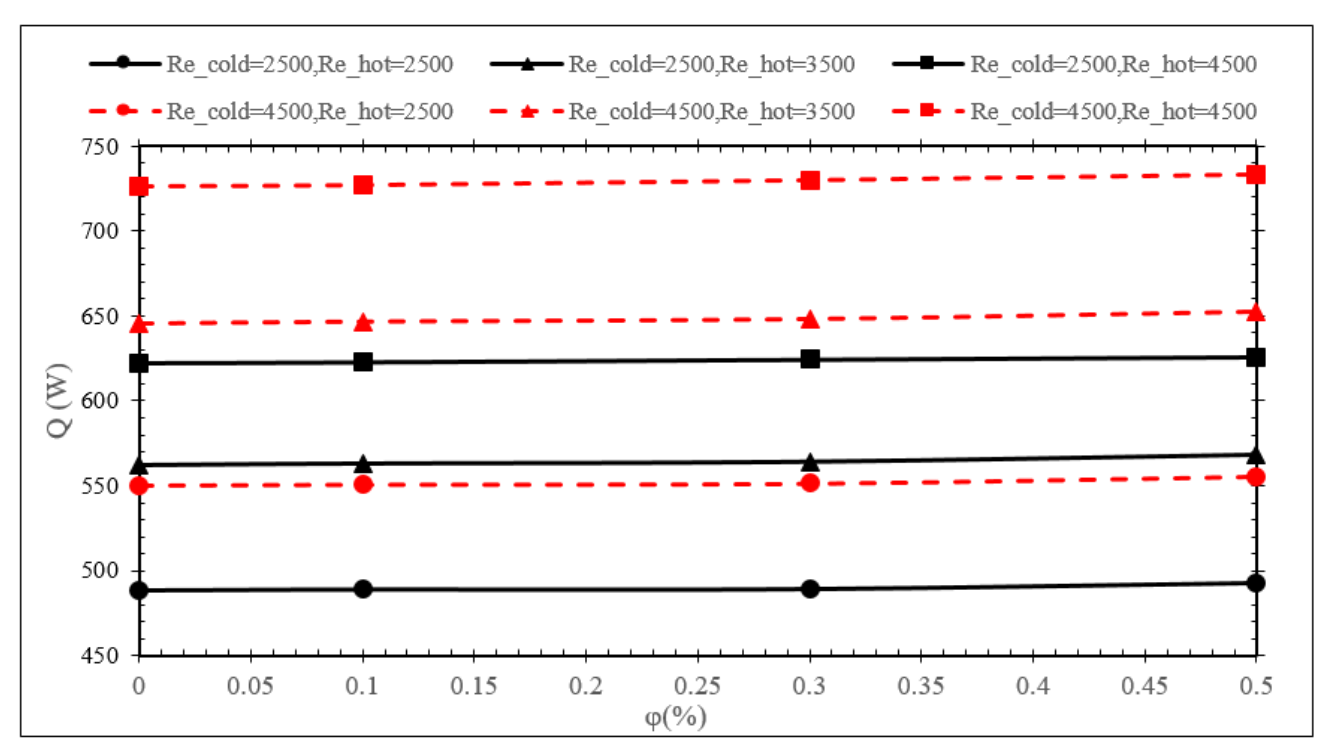


Figure 12. Effect of Al₂O₃-water nanofluid volumetric percentage ratio on heat transfer rate.

The effect of the hot fluid Re number on the Nu is given in Figure 13, and Figure 14 shows the Nu with respect to different Al₂O₃-water volumetric percentage ratio. As seen in Figure 13, the Nu increases with the increase of hot and cold fluid Reynolds numbers. As the Re increases, the turbulence effect increases and U increases, thus the Nu number increases. According to Figure 14, as the φ increased from 0% to 0.3%, Nu number decreased; however, a slight increase occurred between 0.3% and 0.5%. The impact of this trend is less than 1%. With the addition of nanofluid, there is an increase in the thermal conductivity coefficient (K) of the fluid. Although it is expected to decrease because the Nusselt number is inversely proportional to K, the U also has a determining role on the Nu number. According to the definition of Nu= (UxDh)/K, if a sufficient increase in U is not achieved, the Nu number may decrease. On the other hand, increasing viscosity and density of the nanofluid changes U by affecting the development of the boundary layer. In summary, if the increase in K does not provide enough convection effect, it will cause a decrease in the Nu number. However, if the proportional increase in the U is higher than K, an increase in the Nu number may occur. At $\varphi = 0.5\%$ and Rehot= 4500, increasing the Recold number from 2500 to 4500 leads to a 15.6% increase in the Nusselt number. In the numerical study conducted by Yanardag, a similar trend was observed in a microchannel type HEX, which differs from the gyroid HEX studied here. With the addition of higher concentrations of nanoparticles (5% Al₂O₃-water nanofluid) was used, a 309% increase in the Nu number occurred by increasing the Re from 200 to 2500 [23].

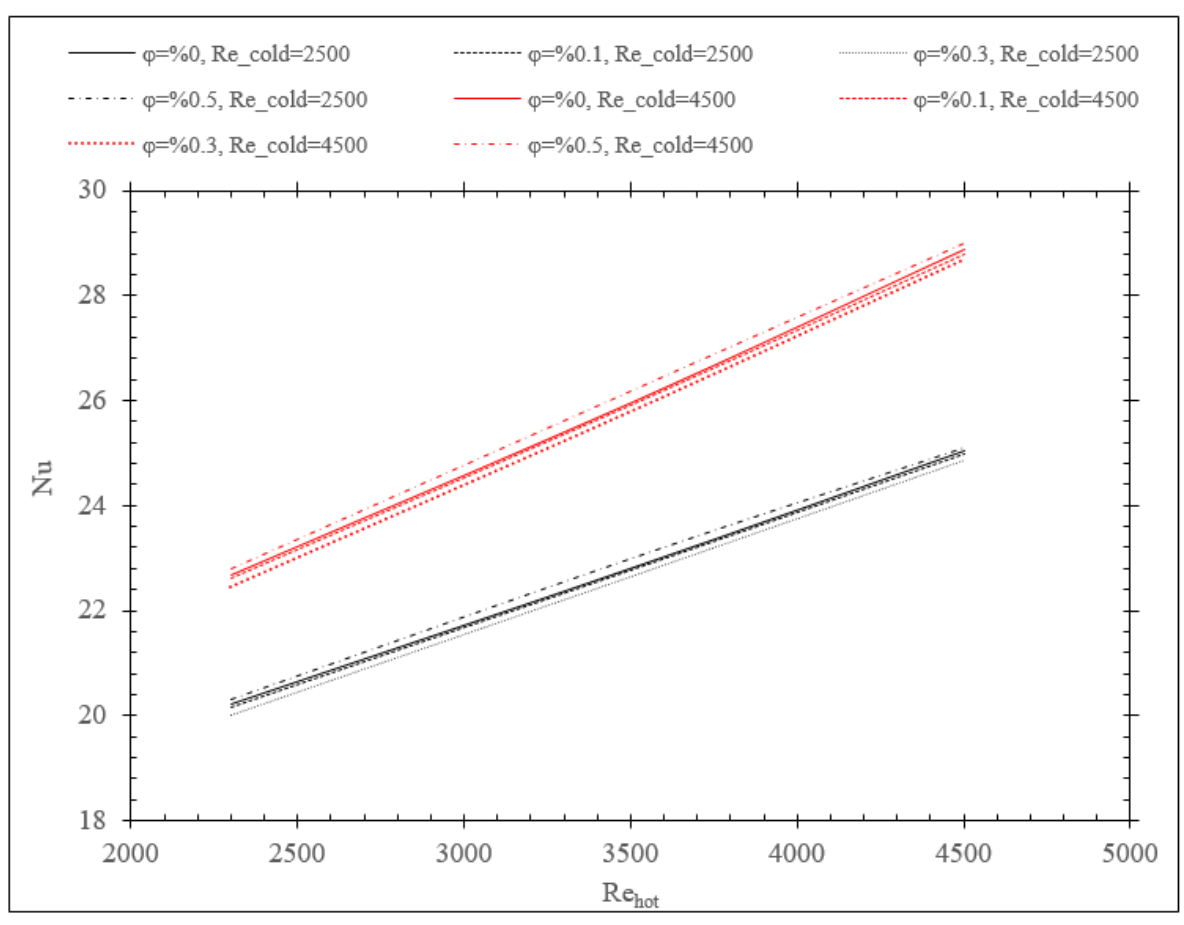


Figure 13. Variation of Nu with respect to Re.

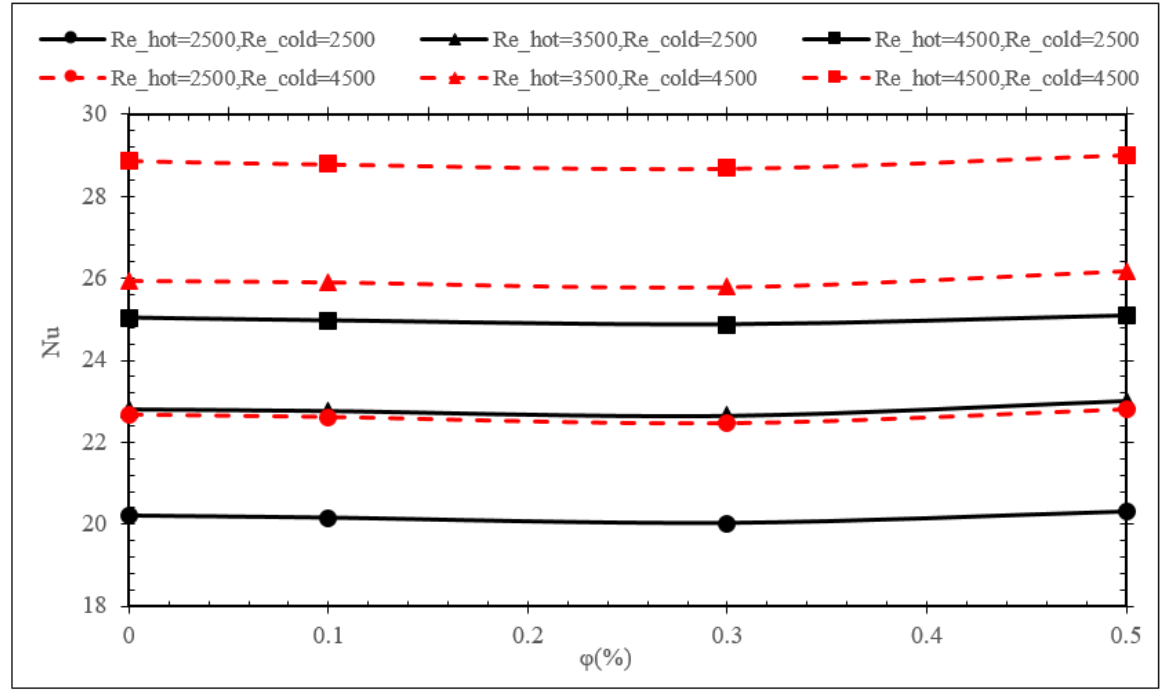


Figure 14. Effect of Al₂O₃-water nanofluid volumetric percentage ratio on Nusselt number.

Figure 15 presents a decrease in the thermal efficiency value between 0-0.3% with the addition of Al_2O_3 nanoparticles in each hot fluid-cold fluid Reynolds combinations, followed by a slight increase in the thermal efficiency percentage between 0.3-0.5% It is seen in the graph that the thermal performance decreases inversely proportionally as the Re value of the hot fluid side increases. Maximum thermal efficiency was observed at conditions Re_{hot} =2500, Re_{cold} =4500.

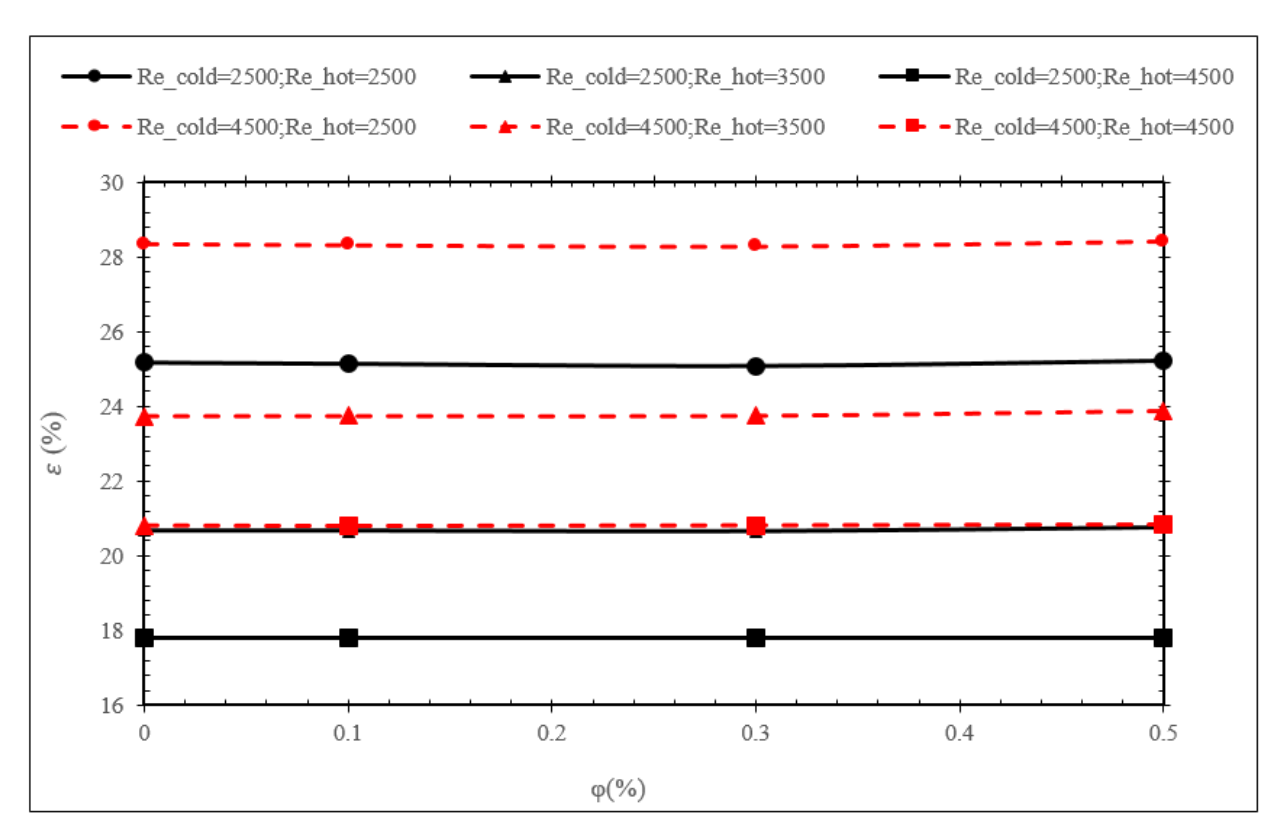


Figure 15. Effect of Al₂O₃-water nanofluid volumetric percentage ratio on efficiency.

4.3. Flow Behavior of Al₂O₃-Water Nanofluid

The results obtained from CFD simulations on the temperature distribution, velocity profiles and flow streamlines of the water- Al_2O_3 nanofluid are evaluated in this section. The temperature distribution contours for different nanofluid volume percentage ratios (%0; 0.1; 0.3; 0.5) at Re=4500 on the cold and hot fluid sides are given in Figure 16(a) and the velocity profiles are given in Figure 16(b). Furthermore, for a comparative evaluation, the flow behavior of 0.3% Al_2O_3 -water nanofluid at two different Reynolds number combinations (Re_{hot}=2500, Re_{cold}=2500 and Re_{hot}=4500, Re_{cold}=2500) was investigated with the contours of temperature distribution and velocity profiles in Figure 17 (a), (b).

A decrease in the temperature of the hot fluid is observed from the inlet to the outlet as a result of effect of the cold fluid as shown in Figure 16(a) and Figure 17(a). The temperature distribution shows that an effective and uniform heat transfer process takes place. It is seen that with the addition of nanoparticles to the base fluid, the temperature gradient decreases and more uniform temperature transitions since the temperature differences of the fluid are stabilize faster. Additionally, with the application of nanofluid, higher temperatures were observed towards the outlet of the HEX. When Figure 17 (a) is examined, it is seen that for $Re_{hot,cold} = 2500$, the heat transfer of the hot fluid along the gyroid structure is at a relatively low and the temperature gradient is sharper; however, in the combination of $Re_{hot}=4500$, $Re_{cold}=2500$, the heat transfer is more effective and there is a significant softening in the temperature gradient due to the effect of the increase in flow rate. In addition, in this combination, it is observed that the temperature near the outlet increases further, and the cold fluid heated more compared to $Re_{hot,cold}=2500$. The directly proportional relationship between heat transfer and flow rate reveals this situation.

As expected from the simulation, it is observed in Figure 16(b) that the vortex formations occur at the same locations within the gyroid structure. In Figure 17(b), when $Re_{cold}=2500$ is kept constant and the Re_{hot} is increased from 2500 to 4500, an increase in the velocity magnitudes around the vortex is observed.

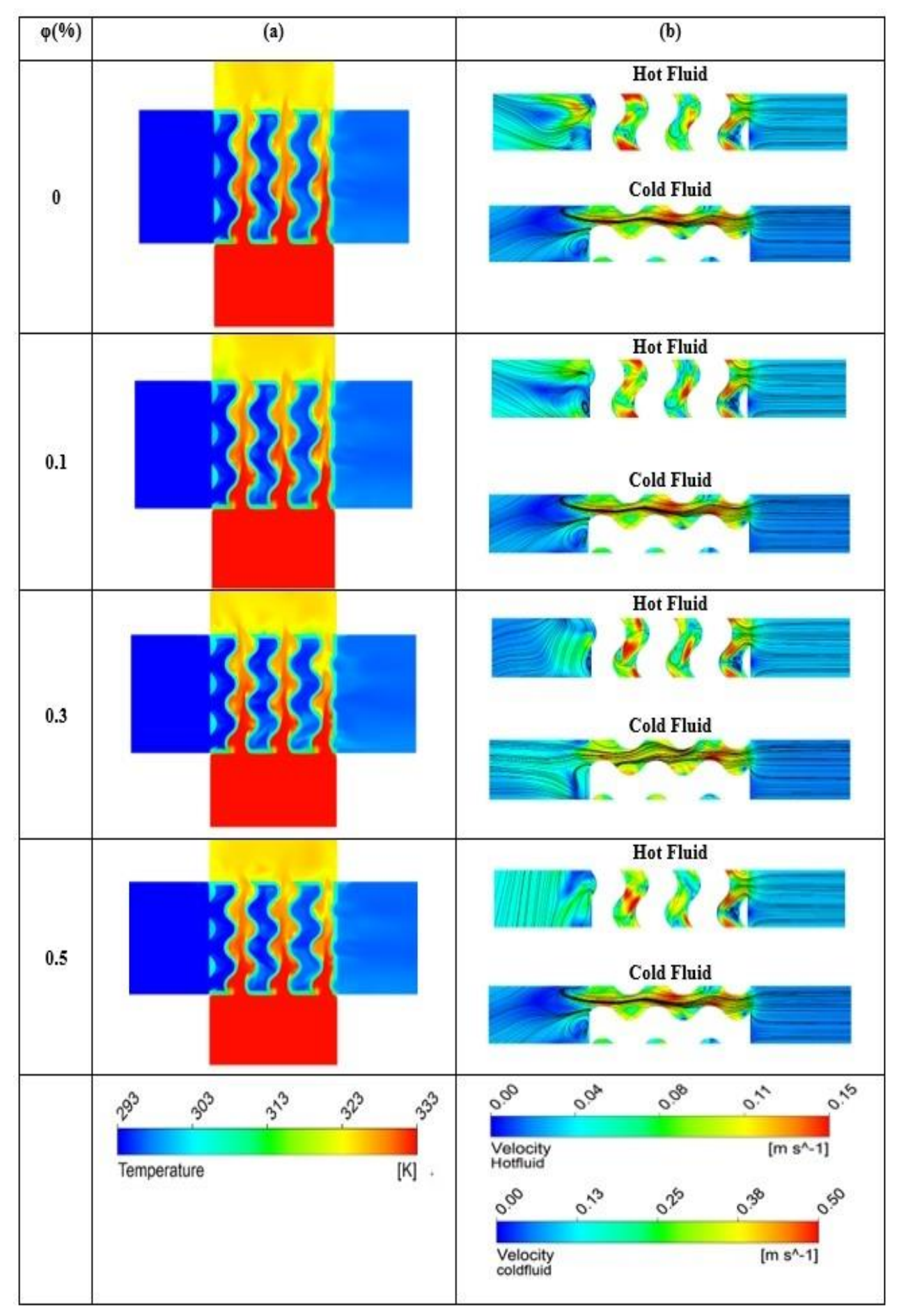


Figure 16. (a) Temperature distribution (b) Velocity and streamline profile at Re_{hot} = Re_{cold} =4500 and 0; 0.1; 0.3 and 0.5% nanofluid volumetric percentage ratios.

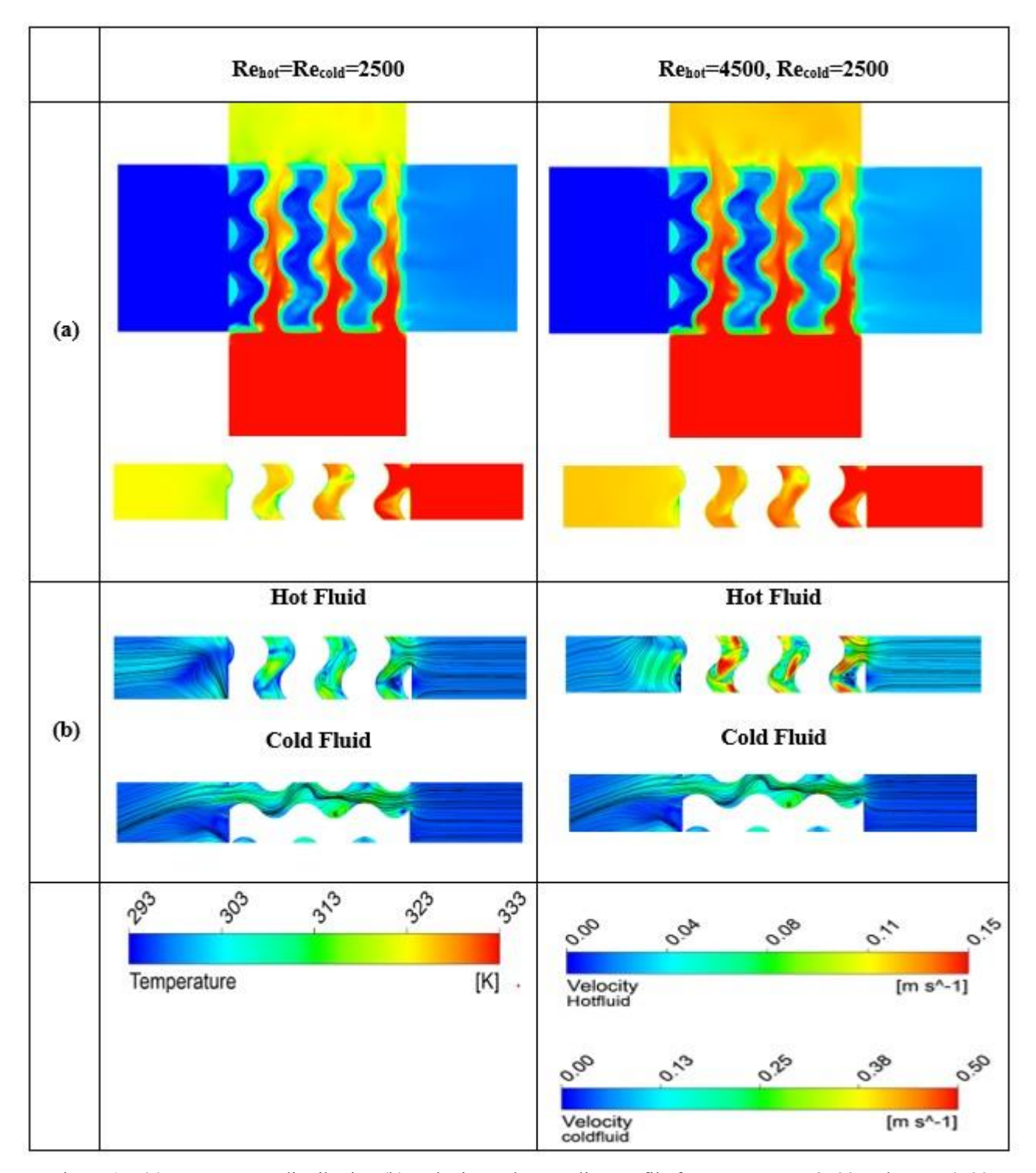


Figure 17. (a) Temperature distribution (b) Velocity and streamline profile for Re_{hot}=Re_{cold}=2500 and Re_{hot}=4500, Re_{cold}=2500 at 0.3% nanofluid volumetric percentage ratios.

4. CONCLUSIONS

The heat transfer characteristics of a gyroid heat exchanger were investigated numerically for two different working fluid configurations: air-air for the cold side and water-water based Al₂O₃ nanofluid. The results are as follows:

• Reynolds numbers of the cold fluid were varied Re_{cold}=2500, 3500, 4500, its relationship with Re_{hot} was examined. It was determined that when Re_{cold} increased, the heat transfer rate and heat transfer coefficient increased in each hot fluid regime. It was observed that the Re_{cold} had an effect on thermal performance similar to the Re_{hot} value. When the (mcp)_{hot}, higher than (mcp)_{cold}, the thermal efficiency decreases. Therefore, the highest performance was obtained under conditions of Re_{hot}=2300, Re_{cold}=4500. The Nusselt number increases for each Re_{hot}-Re_{cold} combination as Re_{cold} increases.

• Analysis study was conducted under conditions of Rehot =2500,3500,4500, Recold=2500,4500 and nanofluid volumetric percentage (0%, 0.1%, 0.3%, 0.5%). As both the nanofluid volumetric concentration and flow rate increased, the heat transfer coefficient and heat transfer rate increased. The Nusselt number increased as Rehot and Recold increased. As the nanofluid concentration increased from 0% to 0.3%, the Nusselt number decreased, but increased slightly between 0.3% and 0.5%. If the increase in the thermal conductivity coefficient does not provide the convection effect sufficiently, it will cause a decrease in the Nusselt number. However, if the proportional increase of the heat transfer coefficient is higher than the thermal conductivity coefficient, an increase in the Nusselt number may occur. At φ=0.5 and Rehot=4500 condition, increasing Recold from 2500 to 4500, the heat transfer increased by 17.1%, heat transfer coefficient and Nusselt number increased by 15.6%. The highest performance was observed in the conditions of Rehot=2500, Recold=4500. While the performance value decreased when the nanofluid percentage was between 0-0.3%, a slight increase between 0.3-0.5% was calculated.

Additionally, TPMS based HEXs, which offer superior thermal performance, may cause challenges in applications such as geothermal or waste heat recovery systems due to their complex internal geometry, especially in environments prone to fouling, clogging, or scaling. In order to overcome such difficulties, it would be useful to develop new designs, optimize channel dimensions according to specific requirements, and to evaluate the manufacturability of these designs with additive manufacturing technology.

Nomenclature

 $\begin{array}{ccc} Re & Reynolds \ number \\ Re_{hot} & Re \ of \ the \ hot \ fluid \\ Re_{cold} & Re \ of \ the \ hot \ fluid \\ Nu & Nusselt \ number \\ \dot{m} & Mass \ flow \ rate, \ (kg/s) \end{array}$

c_p Specific heat capacity, (J/kg·K)

 T_{i} Inlet temperature, (K) T_{o} Outlet temperature, (K) $T_{i,hot}$ T_i of the hot fluid, (K) T_i of the cold fluid, (K) T_{i,cold} T_o of the hot fluid, (K) $T_{o,hot}$ T_o of the cold fluid, (K) $T_{o,cold}$ Hydraulic diameter, (mm) D_h Α Heat transfer area, (m²) μ Dynamic viscosity, (kg/m·s)

ρ Density, (kg/m³) Q Heat transfer rate, (W)

Q_{hot} Heat transfer rate from the hot fluid, (W)
Q_{cold} Heat transfer rate from the cold fluid, (W)

Q_{avg} Avarage heat transfer rate, (W)
Q_{maximum} Maximum heat transfer rate, (W)

ε Thermal efficiency

U Heat transfer coefficient (W/m².K)

K Thermal conductivity coefficient, (W/m·K) V Average flow velocity at flange inlet (m/s)

 ΔP Pressure difference, (Pa) $(\dot{m}c_p)_{hot}$ Flow rate of hot fluid, (kg/m.s) $(\dot{m}c_p)_{cold}$ Flow rate of cold fluid, (kg/m.s) φ Volumetric percentage ratio

HEX Heat exchanger

LMTD Logarithmic temperature difference TPMS Triply periodic minimal surface

REFERENCES

[1] F. Careri, R.H.U. Khan, C. Todd, M.M. Attallah, Additive manufacturing of heat exchangers in aerospace applications: a review, Applied Thermal Engineering 235 (2023) 121387. https://doi.org/10.1016/j.applthermaleng.2023.121387.

- [2] I. Kaur, P. Singh, State-of-the-art in heat exchanger additive manufacturing, International Journal of Heat and Mass Transfer 178 (2021) 121600. https://doi.org/10.1016/j.ijheatmasstransfer.2021.121600.
- [3] S.A. Niknam, M. Mortazavi, D. Li, Additively manufactured heat exchangers: a review on opportunities and challenges, International Journal of Advanced Manufacturing Technology 112 (2021) 601–618. https://doi.org/10.1007/s00170-020-06372-w.
- [4] H. Peng, F. Gao, W. Hu, Design, modeling and characterization of triply periodic minimal surface heat exchangers with additive manufacturing, in: Solid Freeform Fabrication 2019: Proceedings of the 30th Annual International Solid Freeform Fabrication Symposium An Additive Manufacturing Conference, Texas, 2019: pp. 2325–2337.
- [5] D. Liang, C. Shi, W. Li, W. Chen, M.K. Chyu, Design, flow characteristics and performance evaluation of bioinspired heat exchangers based on triply periodic minimal surfaces, International Journal of Heat and Mass Transfer 201 (2023) 123620. https://doi.org/10.1016/j.ijheatmasstransfer.2022.123620.
- [6] D. Liang, K. Yang, H. Gu, W. Chen, M.K. Chyu, The effect of unit size on the flow and heat transfer performance of the "Schwartz-D" heat exchanger, International Journal of Heat and Mass Transfer 214 (2023) 124367. https://doi.org/10.1016/j.ijheatmasstransfer.2023.124367.
- [7] W. Tang, H. Zhou, Y. Zeng, M. Yan, C. Jiang, P. Yang, Q. Li, Z. Li, J. Fu, Y. Huang, Y. Zhao, Analysis on the convective heat transfer process and performance evaluation of Triply Periodic Minimal Surface (TPMS) based on Diamond, Gyroid and Iwp, International Journal of Heat and Mass Transfer 201 (2023) 123642. https://doi.org/10.1016/j.ijheatmasstransfer.2022.123642.
- [8] A. Barakat, Y. Pan, B.B. Sun, Comparative heat transfer performance of TPMS structures: spotlight on Fisch Koch S versus gyroid, diamond and SplitP lattices, in: E3S Web of Conferences ICEMEE 2024, Malaysia, 2024: pp. 1–4. https://doi.org/10.1051/e3sconf/202456001009.
- [9] A. Barakat, B.B. Sun, Controlling TPMS lattice deformation for enhanced convective heat transfer: a comparative study of diamond and gyroid structures, International Communications in Heat and Mass Transfer 154 (2024) 107443. https://doi.org/10.1016/j.icheatmasstransfer.2024.107443.
- [10] S. Samson, P. Tran, P. Marzocca, Design and modelling of porous gyroid heatsinks: Influences of cell size, porosity and material variation, Applied Thermal Engineering 235 (2023) 121296. https://doi.org/10.1016/j.applthermaleng.2023.121296.
- [11] A. Barakat, B.B. Sun, Enhanced convective heat transfer in new triply periodic minimal surface structures: Numerical and experimental investigation, International Journal of Heat and Mass Transfer 227 (2024) 125538. https://doi.org/10.1016/j.ijheatmasstransfer.2024.125538.
- [12] D. Mahmoud, S.R.S. Tandel, M. Yakout, M. Elbestawi, F. Mattiello, S. Paradiso, C. Ching, M. Zaher, M. Abdelnabi, Enhancement of heat exchanger performance using additive manufacturing of gyroid lattice structures, International Journal of Advanced Manufacturing Technology 126 (2023) 4021–4036. https://doi.org/10.1007/s00170-023-11362-9.
- [13] A. Samad, W.H. Lai, Experimental and simulation analysis of heat transfer in gyroid heat exchangers with variable flow channels, International Journal of Heat and Mass Transfer 239 (2025) 126530. https://doi.org/10.1016/j.ijheatmasstransfer.2024.126530.
- [14] G.A. Kilic, Performance evaluation of triply periodic minimal surface heat exchangers using nanofluids at high flow rates for enhanced energy efficiency, Applied Sciences 15 (2025) 4140. https://doi.org/10.3390/app15084140.
- [15] nTop Inc., nTop Release 5.2.2, https://www.ntop.com/, (2025).
- [16] A.H. Schoen, Infinite periodic minimal surfaces without self-intersections (NASA Technical Note TN D-5541, 1970), https://ntrs.nasa.gov/citations/19700020472, (2025).
- [17] B.C. Pak, Y.I. Cho, Hydrodynamic and heat transfer study of dispersed fluids with submicron metallic oxide particles, Experimental Heat Transfer 11 (1998) 151–170. https://doi.org/10.1080/08916159808946559.
- [18] S.-Q. Zhou, R. Ni, Measurement of the specific heat capacity of water-based Al2O3 nanofluid, Applied Physics Letters 92 (2008). https://doi.org/10.1063/1.2890431.
- [19] Y.A. Çengel, A.J. Ghajar, Heat and mass transfer: Fundamentals and applications, McGraw-Hill Education, New York, USA, 2011.
- [20] QED Fusion Materials Database, Alumina (Al₂O₃) material properties, https://qedfusion.org/LIB/PROPS/PANOS/al₂O₃.html , (2025).
- [21] W. Li, G. Yu, Z. Yu, Bioinspired heat exchangers based on triply periodic minimal surfaces for supercritical CO2 cycles, Applied Thermal Engineering 179 (2020) 115686. https://doi.org/10.1016/j.applthermaleng.2020.115686.
- [22] D. Liang, G. He, W. Chen, Y. Chen, M.K. Chyu, Fluid flow and heat transfer performance for micro-lattice structures fabricated by selective laser melting, International Journal of Thermal Sciences 172 (2022) 107312. https://doi.org/10.1016/j.ijthermalsci.2021.107312.
- [23] M. Yanardağ, Numerical investigation of microchannels heat transfer devices by using Nanofluids, Master's Thesis, Gazi University, Graduate School of Natural and Applied Sciences, 2023.